nature ecology & evolution

ARTICLES

https://doi.org/10.1038/s41559-018-0666-4

Seasonal abundance and survival of North America's migratory avifauna determined by weather radar

Adriaan M. Dokter[1]*, Andrew Farnsworth[1], Daniel Fink[1], Viviana Ruiz-Gutierrez[1], Wesley M. Hochachka[1], Frank A. La Sorte[1], Orin J. Robinson[1], Kenneth V. Rosenberg[1,2] and Steve Kelling[1]

Avian migration is one of Earth's largest processes of biomass transport, involving billions of birds. We estimated continental biomass flows of nocturnal avian migrants across the contiguous United States using a network of 143 weather radars. We show that, relative to biomass leaving in autumn, proportionally more biomass returned in spring across the southern United States than across the northern United States. Neotropical migrants apparently achieved higher survival during the combined migration and non-breeding period, despite an average three- to fourfold longer migration distance, compared with a more northern assemblage of mostly temperate-wintering migrants. Additional mortality expected with longer migration distances was probably offset by high survival in the (sub)tropics. Nearctic–Neotropical migrants relying on a 'higher survivorship' life-history strategy may be particularly sensitive to variations in survival on the overwintering grounds, highlighting the need to identify and conserve important non-breeding habitats.

Seasonal animal migrations are events of extraordinary spatial and numerical scale[1,2]. Each year, billions of individuals travel the Earth to reach more suitable areas in which to live and reproduce, often covering astounding distances[1,3,4]. These mass movements constitute biomass exchanges across continents that may profoundly influence multiple facets of ecosystem function, through migrants' roles as competitors, predators and prey, and in transporting nutrients, propagules and pathogens[2]. Migratory behaviour has evolved to exploit seasonal variation in resources and environmental conditions, such that long-distance migrants may benefit from high reproductive output on their resource-rich temperate breeding grounds and from high survival on their tropical overwintering grounds. However, spatiotemporal patterns in mortality and recruitment within migratory bird communities remain poorly understood[5]. In particular, the relative importance of recruitment and overwintering survival in offsetting the costs of presumed higher mortality during the migration journey[6–9] is still unclear. Understanding vital rates across the annual cycle is critical for designing conservation strategies to reverse the steep population declines observed in many migratory bird populations[8,10].

Distributions of migratory bird species are often broad and shift seasonally[11], exposing populations to a complex array of threats and selective pressures[12]. To understand their combined effect on population sizes, we need comprehensive information on demographic rates (for example, mortality and recruitment)[10,13]; however, this information is challenging to obtain at relevant spatial and temporal scales. Population monitoring programmes[7,14] and tracking studies on larger-bodied birds[6] have provided estimates of baseline vital rates for a few bird species at various points in their annual cycles. Yet, these studies are highly local, labour intensive, and yield widely varying estimates of survival and reproductive rates within and across species and sites[15]. Therefore, generalization of current results to broader geographic areas and larger species assemblages can be problematic[10,13]. Recruitment data are equally challenging to collect, especially recruitment into the migratory population after birds have dispersed out of researchers' breeding-ground study areas. Nevertheless, consensus is emerging that mortality rates during migration are higher than in any other period of the annual cycle[7–9], with the most direct evidence from larger-bodied species[6,16] and larger uncertainty remaining for small songbirds[9,17]. Because longer-distance migrants presumably have greater exposure to risks and challenges of migration, we expect a lower proportion of their population to return from their overwintering grounds than shorter-distance migrants, unless high survival rates at their distant overwintering grounds offset mortality during migration.

We tested these expectations regarding seasonal changes in biomass for migratory birds in North America using an existing network of weather surveillance radars[18] distributed across the contiguous United States. Data from this radar network provide a unique and unprecedented opportunity for quantifying continent-wide patterns of animal movements and abundances[19]. Because radar networks operate continuously, have continental-scale coverage, and provide velocity and biomass density measurements in a highly standardized manner, they can provide quantitative large-scale estimates of biomass transport in the atmosphere (see Methods). However, until recently, obtaining and analysing radar data has been prohibitively time consuming[19], precluding continent-wide analyses.

Recently, the National Oceanic and Atmospheric Administration and Amazon Web Services (AWS) Cloud made available one of the largest datasets describing animal movement ever compiled[20]: the Next Generation Weather Radar (NEXRAD) archive. The NEXRAD network contains 143 WSR-88D weather radars in the contiguous United States (Figs. 1 and 2)[18], which since 2013 have collected dual-polarization data. Here, we used established methods to extract vertical profiles[21] of the density, speed and direction (Supplementary Fig. 1) of nocturnally migrating birds from 2013–2017 for all 143 radars in the network. By combining data across all radars, we provide estimates of total migratory biomass transport across the

[1]Cornell Lab of Ornithology, Cornell University, Ithaca, NY, USA. [2]American Bird Conservancy, Washington DC, USA. *e-mail: amd427@cornell.edu

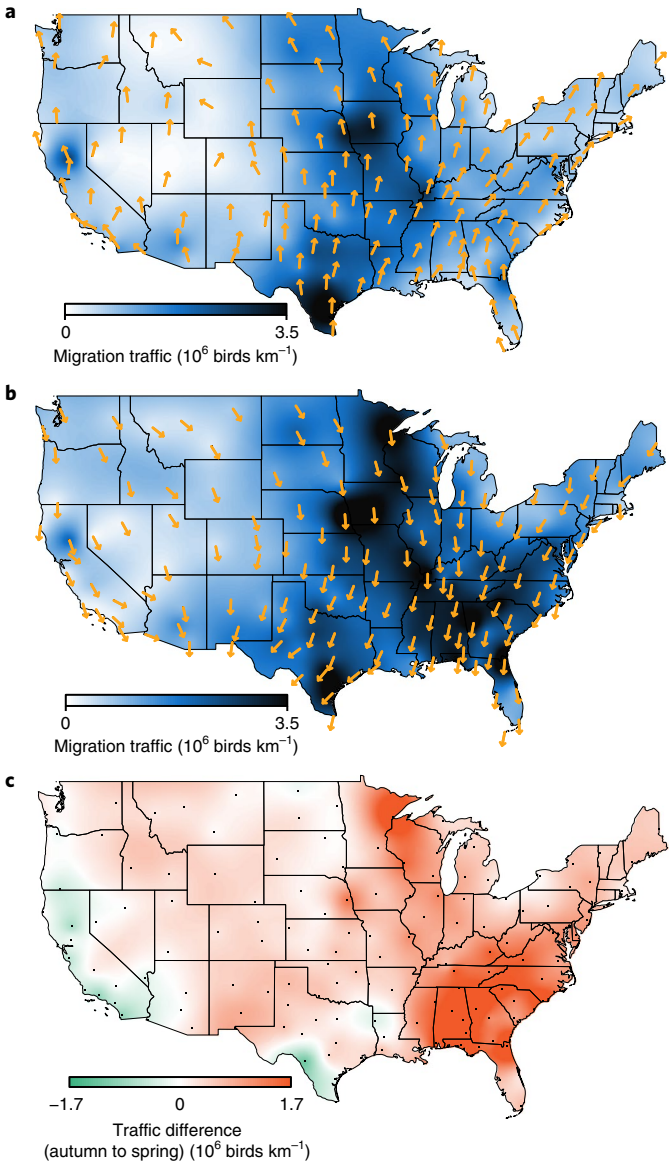

Fig. 1 | Cumulative nocturnal migration traffic in spring and autumn. **a**,**b**, Migration traffic (logarithmic colour scale) in spring (1 March to 1 July; **a**) and autumn (1 August to 1 December; **b**) averaged over five years (2013–2017). Orange arrows indicate the seasonally averaged directions of migration. **c**, Difference in migration traffic between spring and autumn. Orange and green colours indicate higher autumn and spring biomass passage, respectively. Migration passage was higher in autumn in most areas due to the new cohort of juveniles after reproduction. In spring, biomass passage peaked in the central United States, while in autumn migration was more easterly, with high traffic above the Appalachian Mountains and eastern Gulf of Mexico. Higher spring passages in California and Texas indicate looped migratory pathways that are more westerly in spring. See Supplementary Videos 1–4 for animated versions.

continental United States, and by comparing total biomass flows during spring and august migrations, we gain insights into assembly-wide demographic processes affecting the entire North American migratory avifauna.

Results

We found considerable spatial and seasonal variation in migration pathways across the contiguous United States (Fig. 1), reflecting both shifts in migration routes and demographic changes in total bird biomass detected across radar stations. In spring (1 March to 30 June), migration was concentrated throughout the central United States (Fig. 1a and Supplementary Videos 1 and 3). In autumn (1 August to 30 November), the average migration pathway shifted eastward (Fig. 1b,c and Supplementary Videos 2 and 4) and divided at the Gulf Coast, with an eastern pathway crossing the Gulf of Mexico and a western pathway circumventing the Gulf through Mexico (Fig. 1b). The eastward shift in migratory passage from spring to autumn is consistent with looped migrations[11,22] driven by seasonal patterns in wind and food availability.

To measure the total migratory passage into and out of the contiguous United States while controlling for the effect of seasonally shifting pathways, we delineated two coast-to-coast transects across the northern and southern United States borders (Figs. 2–4). These transects acted as continent-wide gateways for quantifying migratory passage (biomass abundances and timing) that, owing to the cross-continental extent, are insensitive to seasonal variation in the longitudinal location of migration pathways.

Our quantification of migration passages reveals a continental exchange of several billion birds across the two transects (Fig. 2 and Supplementary Table 1). Across the northern transect, the biomass equivalent of 3.97 ± 0.17 billion (mean ± s.d. over years) passerine-sized birds migrated southward in autumn and an equivalent of 2.56 ± 0.11 billion birds returned northward in spring. Across the southern transect, 4.72 ± 0.19 billion passerine-sized birds migrated southward in autumn and 3.55 ± 0.07 billion birds returned northward in spring. Our radar-based estimates are of the same order of magnitude as several indirect estimates for continental-scale exchanges based on estimated population sizes of breeding birds. Using Partners in Flight (PIF) population size estimates, and breeding and overwintering ranges of migratory landbirds[23,24], we estimate that 2.5 billion (south transect) to 2.7 billion (north transect) landbirds migrate into and out of the contiguous United States in spring (see Methods). On the same order of magnitude, in the Palaearctic–African migration system, 2.1 billion landbirds were estimated to migrate from Europe into Africa in autumn[1].

We calculated return ratios of spring to autumn passage, $\phi_{s/a}$, across each transect—proportions that indicate the net loss of biomass due to mortality in the non-breeding period, lasting from the autumn transect passage to the subsequent spring passage. Across the northern transect, the return proportion was $\phi_{s/a} = 0.64 \pm 0.06$ (mean ± s.d. over 5 years; Fig. 2b and Supplementary Table 2). Across the southern transect, the return proportion was $\phi_{s/a} = 0.76 \pm 0.03$, which is significantly higher than that for the northern transect (Wald $\chi^2(1) = 16.4$, $n = 4$, d.f. = 1, two-tailed $P < 0.001$). This difference in return proportions (that is, between $\phi_{s/a}$ and $\phi_{a/s}$) remained significant after converting to temporal rates (that is $\widetilde{\varphi}_{s/a}$ and $\widetilde{\varphi}_{a/s}$; see Methods; $\chi^2(1) = 9.2$, $n = 4$, d.f. = 1, $P = 0.002$) to account for differences in the time birds spent south of each transect (228 ± 2 days in the northern transect and 207 ± 2 days in the southern transect; Fig. 3, Supplementary Fig. 2 and Supplementary Tables 1 and 2).

In a similar manner, we calculated the ratio of autumn biomass passage to the previous spring passage as an index of recruitment into the migratory population, accounting for both reproductive output and subsequent mortality during the post-breeding and early august migration periods. For the southern transect, this estimate ($\phi_{a/s} = 1.36 \pm 0.04$) shows that for each northward migrating adult only an additional 0.36 recruits are added to the southward migrating population. A larger (Wald $\chi^2 = 46.0$, $n = 4$, d.f. = 1, two-tailed $P < 0.001$) additional biomass returned across the northern transect ($\phi_{a/s} = 1.60 \pm 0.09$), representing an additional 0.60 recruits added to the southward migrating population for every adult bird heading north the previous spring.

To account for birds that might bypass the southern transect in autumn due to a more easterly transatlantic migration route, we also quantified the passage of birds that may be departing off

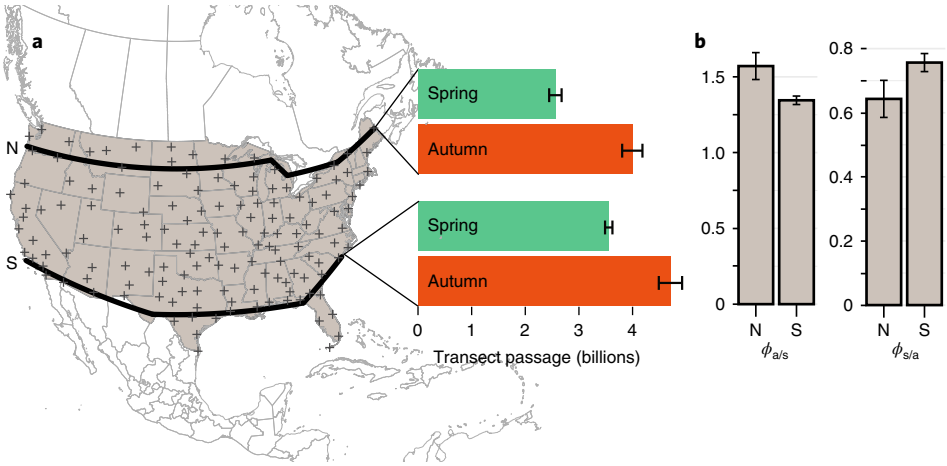

Fig. 2 | Southern and northern transects for quantifying seasonal biomass passage, migration traffic across these transects, and associated demographic indices. a, Seasonal cumulative migration traffic across the transects in spring (green bars) and autumn (red bars). Thick black lines indicate the southern and northern transect for quantifying seasonal biomass passage. Plus signs indicate the location of radar stations. **b**, $\phi_{a/s}$ is the ratio of autumn transect passage over the preceding spring passage, representing a demographic index of recruitment into the migratory period. $\phi_{s/a}$ is the return of spring passage over the preceding autumn passage, an index of mortality occurring south of the transect. Error bars indicate the interannual variation across the study years expressed as s.d.

the Atlantic coast, using an additional transect running from the easternmost tip of the northern transect to the easternmost tip of the southern transect (Maine to North Carolina). We found that, in autumn, a biomass equivalent of 219 ± 63 million birds crossed this coastal transect towards the southeast. In spring, the net passage across this coastal transect was also eastward, equalling 63 ± 12 million birds. In the unlikely scenario that all birds crossing this coastal transect bypass the southern transect only in autumn but not in spring (in a looped migration), this would lead to an overestimation of the southern transect return rate $\phi_{a/s}$ by 4%. Accounting for this potential bias did not change the significance of the difference in return rate between the northern and southern transect. However, we note that even though looped migration is common in eastern North America, most birds that migrate in a looped trajectory do not perform transatlantic migration in autumn[11], and the number of species—especially passerine species—bypassing the southern transect in autumn is probably very small[25].

Birds crossing the northern and southern transects differ in species composition and the total distance required to complete their migration journey (see Fig. 3), which we estimated using independent distribution maps and breeding population estimates (see Methods and Supplementary Information). Passage across the northern transect was dominated by shorter-distance migrants with an assembly-averaged overwintering area located around 400 km south of the transect (still well within the contiguous United States). In contrast, the assemblage crossing the southern transect was dominated by longer-distance migrants whose overwintering area was located around 1,400 km south of the transect, on average. Body size distributions of landbird species passing the transects were similar for the two assemblages (17 ± 13 g for the north transect and 17 ± 14 g for the south transect; weighted *t*-test by species population size: $t = 0.288$, d.f. = 311, $P = 0.8$; see Supplementary Information). Based on the same distribution maps and breeding population size data, we estimate that at least 19%, and at most 40%, of all migrants crossed both transects. The assemblages represented at the two transects are thus partly overlapping.

Discussion

Our finding that the return rate of biomass from autumn to spring was higher across the southern transect than at the northern transect has a surprising implication: cumulative mortality experienced during migration and the overwintering periods was significantly lower for birds migrating towards the Neotropics than for birds overwintering in the temperate United States, despite a greater average migration distance remaining for birds crossing the southern transect. Therefore, longer migration distances did not result in higher relative biomass loss and lower spring return rates, suggesting that high overwintering survival in the tropics might be compensating for the increased mortality presumably associated with longer migration. Alternatively, a higher return rate across the southern transect could result from latitudinal variation in migration mortality if mortality during migration at (sub)tropical latitudes is substantially lower than at temperate latitudes. Although mortality has not been quantified at different points in the migration route, the 'latitudinal variation in migration mortality' explanation seems unlikely as southern latitudes include major ecological barriers to migration; for example, Mexican arid zones and the Gulf of Mexico, which are thought to be dangerous to cross[26]; however, note the specific challenges in highly industrialized landscapes described below.

In stable populations, opposite patterns of recruitment would be necessary to compensate for differences in mortality rates of temperate- and southern-wintering birds. We found that at the northern transect the number of recruits added to the migratory population was significantly higher (0.60) than at the southern transect (0.36). This contrast between northern and southern transects is consistent with latitudinal increases in clutch size[27] and a higher fecundity of shorter-distance migrants compared with long-distance migrants[28,29]. Because average migration distance (and associated mortality during migration) north of the two transects was similar (1,396 versus 1,510 km), our return rates probably indicate that latitudinal increases in clutch size and fecundity resulted in higher numbers of fledglings produced, thus increasing recruitment into the migratory population at more northern latitudes.

Our radar-derived demographic indices are inherently seasonal, spanning clearly defined portions of the annual cycle. Very few studies have so far quantified seasonal demographic rates away from breeding grounds[8], and estimates are available for only a handful of migratory species[7,9]. Published estimates come from long-term studies of simultaneously monitored populations on breeding and wintering areas for highly site-faithful species[7–9], as well as satellite tracking studies on larger-bodied birds[6]. The latest full annual cycle population models for small passerines suggest very high adult

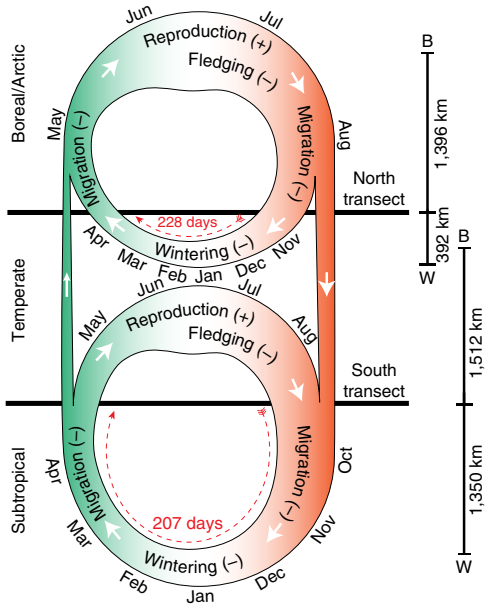

Fig. 3 | Annual cycle of avian biomass flow across the north and south transect. Segment widths represents the amounts of biomass of the avian assemblages associated with the two transects. Distance markers on the right indicate the average distance from the breeding (B) and wintering (W) area for the assemblage of birds crossing each transect, respectively. Monthly labels indicate the progression of time (time is not proportional to the length of the segments). (+), (–) indicate biomass growth, loss, respectively.

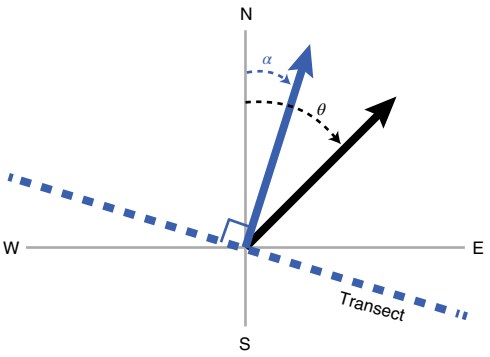

Fig. 4 | Angular definitions of transect direction and bird ground speed direction. The transect is displayed as a dashed line. The direction of the transect is given by the angle α defined relative to the blue arrow perpendicular to the transect, whose value is limited to the −90° to +90° range. The black arrow gives the ground speed vector of migration, with the direction θ.

survival during stationary periods on the wintering grounds in the Neotropics[7–9]. Our observation of a relatively high spring return $\phi_{s/a}$ at the southern transect provides continent-wide evidence of higher survival among the full assemblage of Neotropical migratory birds south of the United States, which potentially offsets higher expected mortality rates during migration[6,7,9,16] compared with the combined non-breeding and migration survival of shorter-distance temperate-wintering migrants.

Relative to the number of fledglings produced by most migratory landbirds (around 1–2 per capita[1,28,29]), our recruitment indices indicate that per northward migrating adult in spring, relatively few recruits are added to the migratory population in autumn (0.36 at the southern transect and 0.6 at the northern transect). These numbers suggest a major loss of biomass through mortality even before the transects are reached, which is also consistent with high mortality rates during the immediate post-fledging period, as observed in numerous species-specific studies[15,30–32] and during migration.

We suggest that differences in mortality and recruitment rates observed between the two transects are primarily related to general differences in life-history strategies among their associated species assemblages, including a broad range of adaptations to climate, vegetation types and food resources that vary according to the latitude of breeding and non-breeding distributions. From a life-history perspective, our results suggest that, on average, birds overwintering south of the United States showed a 'higher survivorship' strategy, while migrants overwintering in the temperate zone tended towards a 'higher recruitment' strategy. Life-history strategies relying on high survivorship are more sensitive to perturbations in adult survival rates in non-breeding areas[33]. Thus, even though birds overwintering south of the United States had an overall higher return rate than temperate-wintering birds, their populations may be more sensitive to perturbations in adult non-breeding survival, emphasizing the need to monitor survival rates of birds outside the breeding areas, especially within the Neotropics.

As unprecedented anthropogenic changes in land use and climate strongly impact ecosystems and organisms worldwide[34], migratory birds in particular are suffering widespread population declines[10,13]. Large-scale demographic patterns in mortality and recruitment may no longer reflect environmental conditions under which life-history strategies of migrants evolved. In highly industrialized countries such as the United States, migrants face new sources of direct mortality from anthropogenic causes; for example, collisions with structures (sometimes mediated by the effects of artificial light[35,36]) or predation by cats[37], potentially decreasing survival in temperate (more urbanized) latitudes. Indirect effects of climate change and human-induced habitat degradation affect migrants throughout the annual cycle, with habitat loss accelerating especially at tropical latitudes[38]. Understanding and mitigating the effects of global change and human activity on demographic rates will be crucial for conservation. Our study illustrates how meteorological radar infrastructure can provide a baseline of seasonal abundances and return rates for the entire migratory bird assemblage of North America, which can be monitored for years and decades to come as conditions along flyways continue to change.

In summary, by taking advantage of an existing meteorological radar infrastructure, our study provides baseline information on seasonal passages of bird biomass across the contiguous United States. We used these data to calculate continental-scale demographic indices that indicate average differences in mortality and recruitment rates between assemblages of migratory birds overwintering predominantly within the United States and birds spending the non-breeding season predominantly in the Neotropics. These indices offer a benchmark for putting species-specific studies into a more general context, and an unprecedented opportunity to track and assess shared drivers of population change for billions of migratory birds simultaneously. Our findings indicate a 'higher survivorship' strategy used by longer-distance migrants spending the northern winter south of the United States, with an emphasis on high adult survival within Neotropical non-breeding grounds. For birds that rely on high survival to offset the risks of long-distance migration, even small reductions in habitat quality can potentially drive population declines, as observed in many Neotropical migratory species. Understanding how global change is likely to affect non-breeding habitats, where these migrants spend the majority of the annual cycle[38], will be critical for preserving this hemispheric migration system.

Methods

Extraction of vertical profiles of birds. We extracted vertical profiles of bird speeds, directions and densities (see Supplementary Fig. 1a) using the algorithm

vol2bird (version 0.3.15)[21], which is available on GitHub (https://github.com/adokter/vol2bird). We briefly describe the main processing steps and study-specific settings.

Vertical altitude bins were defined relative to sea level in 200 m height intervals up to 4 km altitude. We removed meteorological signals based on high correlation coefficient values (>0.95) provided in the dual-polarization radar data (which indicate the temporal autocorrelation of the vertically and horizontally polarized components of the detected signal by the radar)—a highly reliable polarimetric indicator of precipitation[39,40]. Polarimetric data are only available since 2013 upgrades to US radars, which is why we restricted our analyses of NEXRAD S-band data to the 4.5 years of available dual-polarization data.

A cell-searching algorithm detected contiguous cells of high correlation coefficients, defining cells as groupings of sample volumes within an elevation scan for which each sample volume has a correlation coefficient greater than 0.95, and at least 5 directly neighbouring sample volumes (in a Moore neighborhood sense) that also meet this requirement. We removed only data from contiguous precipitation cells of 0.5 km^2 or larger, to retain the occasional speckle of high correlation coefficient sample volumes found in bird migration areas. We added an additional buffer of 5 km width around the selected precipitation cells to effectively remove the borders of precipitation areas, which tend to have less well-defined correlation coefficient values, thus limiting the risk of precipitation contaminations[21].

We produced static beam blockage maps for all weather radar sites following Krajewski et al.[41]. We excluded all sectors from the analysis for areas with (partial) beam blockage based on surrounding topography, as obtained from a 100-m-resolution topographical map provided by the US Geological Survey[42], and assuming a 1° beam width. We assumed a standard refraction of the beam towards the Earth's surface by using an effective Earth's radius of 4/3 × (true radius)[43]. From this topographical map, we also extracted the minimum, mean and maximum ground level within a 25 km radius of each radar (Supplementary Table 5). For radars with a minimum ground level below the antenna height, we extrapolated migration estimates for the lowest bin (at antenna level) down to 400 m below the antenna level. At even lower altitudes, the radar was considered blind, which mainly applied to some radars in the central Rocky Mountains, away from the transects used for counting bird passages (see Supplementary Table 5).

An additional dynamic clutter map was used to exclude sample volumes with a Doppler velocity in the interval of −1 to 1 m s^{-1}, to filter out ground echoes associated with anomalous beam propagation[43] and other clutter from other remaining static ground targets. We used sample volumes in the 5–35 km range only, which excludes the closest sample volumes with a high probability of ground clutter contamination and maintains a narrow beam width that can resolve the altitudinal distribution of birds. The processing steps described below were conducted only on the sample volumes that remained after exclusion of precipitation and ground clutter.

We de-aliased radial velocities using a torus mapping method[44], which is also used in the product generation framework of the European Operational Programme for the Exchange of Weather Radar Information (OPERA) network, as well by meteorologists in the Baltrad weather radar network for the Baltic sea region[45]. This method de-aliases velocities using a fit to a linear velocity model that is wrapped at the Nyquist velocity of each scan, very similar to a de-aliasing technique[46] applied earlier in bird migration studies using North American NEXRAD radars. We applied separate de-aliasing of each altitude layer of interest, which may contain sample volumes of different elevation scans. In the de-aliasing fit, we took into account each of the (potentially different) Nyquist velocities of the elevation scans.

We extracted speed and direction estimates from the de-aliased velocity fields using the volume velocity profiling (VVP) technique[21,47,48]. Weather radar reflectivity factor values (dBZ) were converted to reflectivity ($cm^2 km^{-3}$), and for each altitude layer the geometric mean reflectivity η over all sample volumes in the altitude layer was calculated. Reflectivity can be expressed as bird numbers using an estimate of the average radar cross-section (RCS) of an individual migrating bird. Here, we used a yearly mean RCS of 11 cm^2 for an individual bird, determined in a calibration experiment spanning a full spring and autumn migration season[21]. This value corresponds to passerine-sized birds (10–100 g range)[49], which represents the highest-abundance species group dominating our radar signals (Supplementary Fig. 5; Supplementary Table 3 and Methods).

The vol2bird algorithm finally removes altitude layers with radial velocity standard deviations $\sigma_{VVP} < 2$ m s^{-1}, with σ_{VVP} a measure of radial velocity texture, defined as the root of sum of the residual squared errors between the radial velocity data and the VVP velocity model. This radial velocity texture represents an additional filter for cases of precipitation, and wind-drifting insects that cause smooth velocity fields that represent the wind. Birds, however, have active and highly variable self-speeds[21], causing high spatial variability in radial velocities.

We accessed NEXRAD weather radar data from the public 'noaa-nexrad-level2' Amazon S3 bucket[20]. We containerized a pipeline for downloading and processing these data using Docker[50], and deployed this in the AWS Cloud using the AWS Batch service (https://aws.amazon.com/documentation/batch/). Cloud computing reduced this computation task of 14,000 central processing unit (CPU) hours to less than a day.

Migration traffic from vertical profile time series. The vertical profiles of single radars make up time series, which we used to calculate the cumulative seasonal passage of migratory birds for each individual radar. Our analysis focuses on nocturnal migration, which is by far the most common migratory strategy because it is highly time and energy efficient[51]. We first calculated the migration traffic rate (MTR) for each nocturnal profile in the time series (see Supplementary Fig. 1b), which is a flux measure defined as the number of targets crossing a 1 km transect per hour (in individuals $km^{-1} h^{-1}$; see Fig. 4 for definitions of the angles in relation to ground speed and transect direction). For a transect always kept perpendicular (⊥) to the migratory ground speed direction, MTR is always a positive quantity, defined as:

$\mathrm{MTR}_{\perp,t} = \sum_i \rho_{i,t}\, v_{i,t} \Delta h$, where t is an index of time, $\rho_{i,t}$ is the bird density at altitude layer i (in km^{-3}), $v_{i,t}$ is the bird ground speed at altitude layer i (in km h^{-1}) and Δh is the width of the altitude layers (0.2 km). MTRs can also be calculated for transects with a fixed direction, α (see Fig. 4), in which case the number of crossing targets per hour per km of transect is calculated as:

$\mathrm{MTR}_{\alpha,t} = \sum_i \rho_{i,t} v_{i,t} \cos[\vartheta_{i,t} - \alpha] \Delta h$, where $\vartheta_{i,t}$ is the migratory direction at altitude bin i and time index t. Note that this equation evaluates to the previous equation when $\alpha = \vartheta_{i,t}$, as required. In this definition, MTR_α defines the flux of birds in a direction of interest. Targets moving northward over the transect contribute positively to MTR_α, while targets moving in southward directions contribute negatively to MTR_α. Therefore, MTR_α can be either positive or negative, depending on the direction of migration θ. As an additional quality control, we only included $\rho_{i,t}$ when θ was in the southward semicircle surrounding a radar station in autumn and when θ was in the northward semicircle in spring. As we define directional angles clockwise from north, MTRs in spring were positive and MTRs in autumn were negative.

The MTR values of individual profiles were further aggregated into values of cumulative night-time migration traffic (in individuals km^{-1}):

$$\mathrm{MT}_\perp(T_{\mathrm{start}}, T_{\mathrm{end}}) = \sum_{t=T_{\mathrm{start}}}^{T_{\mathrm{end}}} \mathrm{MTR}_{\perp,t} \Delta t$$

$\mathrm{MT}_\alpha(T_{\mathrm{start}}, T_{\mathrm{end}}) = \sum_{t=T_{\mathrm{start}}}^{T_{\mathrm{end}}} \mathrm{MTR}_{\alpha,t} \Delta t$, where Δt is the time difference between consecutive profiles in hours. Profiles were calculated at half-hour intervals for each radar during night time only, selecting the profiles closest to 0 and 30 min for each hour. A 30 min time interval was found to be optimal for balancing computational efficiency and accuracy of the results. A test run on a subset of 18 radars for 3 years at the full available temporal resolution (around 5–10 min) showed that down-sampling to 30 min produced estimates of migratory passage migration traffic that were within 1% of the original.

In calculations of seasonal migration traffic, the spring season was taken to be from 1 March to 31 June; that is, T_{start} equalled the index of the first profile of March and T_{end} the index of the last profile in June. The autumn season was taken to be 1 August to 31 November; that is, T_{start} equalled the index of the first profile of August and T_{end} the index of the last profile in November. Figure 1 shows plots of the spatial interpolation of $\mathrm{MT}_\perp$ calculated for the autumn and spring seasons (see next paragraph for interpolation methods).

Seasonal transect passage. We chose the northern and southern transects to minimize orographic obstructions. A few radars in the central Rocky Mountains are located on higher mountains, which makes these areas less suitable for coast-to-coast transects, as some migrations may pass below the field of view of the radar. We selected the radar stations to use for the northern and southern transects because their radars were relatively free from such topographic effects (see Supplementary Table 5), and their transect segments were chosen to roughly follow the northern and southern border of the United States. Each transect consists of multiple line segments, each with a line segment direction α_j of constant course. The north transect largely follows 46° N latitude, defined by straight line segments in Mercator projection between locations 46° N/124° W, 46° N/85° W, 44° N/83° W, 44° N/75° W and 46° N/67.78° W. The south transect largely follows 30° N latitude through locations 34° N/120° W, 30° N/103° W, 30° N/84° W and 34° N/78° W. An additional coastal transect was defined from the easternmost tip of the northern transect to the easternmost tip of the southern transect; that is, from 46° N/67.78° W to 34° N/78° W. To calculate migratory passage over a line segment, we first calculated seasonal migration traffic MT_{α_j} for all radars. Spatial interpolations of seasonal migration traffic were generated using ordinary kriging in the R package gstat[52]. We clipped water areas after interpolating, leaving land areas of the contiguous United States. A small section of the transect in the north-east runs over Canadian territory and the Great Lakes, and we extended interpolations of migratory movements into this area when calculating transect passages. Finally, we integrated the migration traffic values (in individuals km^{-1}) over the length of the line segment, giving the total migratory passage of individuals for that line segment. These calculations were repeated for all line segments of a transect, and the total transect passage was calculated as the sum of the migratory passage over all segments.

For each radar, we calculated the mean passage date of birds into the direction α as:

$$t_\alpha(T_{\mathrm{start}}, T_{\mathrm{end}}) = \frac{\sum_{t=T_{\mathrm{start}}}^{T_{\mathrm{end}}} t\ \mathrm{MTR}_{\alpha,t} \Delta t}{\sum_{t=T_{\mathrm{start}}}^{T_{\mathrm{end}}} \mathrm{MTR}_{\alpha,t} \Delta t}$$

Supplementary Fig. 2 shows the spatial variation in mean transect passage date in spring and autumn $t_\perp$ (keeping α parallel to the migratory direction θ as in $MT_\perp$). Values of t_α were spatially integrated and summed over the line segments of transects as for MT_α into seasonal mean transect passage dates t_{pass}, and summarized in Supplementary Table 1.

We calculated the transect parameter $\phi_{s/a}$ as the spring passage over the preceding autumn passage, and $\phi_{a/s}$ as the autumn passage over the preceding spring passage. These ratios do not depend on the assumed RCS factor converting reflectivity to bird numbers, as they are a biomass ratio for which RCS cancels in division. The parameters $\tilde{\varphi}_{s/a}$ and $\tilde{\varphi}_{a/s}$ are the same ratios expressed as return rates per month, which take into account the average time passed between the autumn and spring passages, as in:

$\tilde{\varphi}_{s/a} = \phi_{s/a}^{\frac{1}{(t_{pass,s} - t_{pass,a})} \frac{365}{12}}$

$\tilde{\varphi}_{a/s} = \phi_{a/s}^{\frac{1}{(t_{pass,a} - t_{pass,s})} \frac{365}{12}}$, with the mean spring and autumn transect passage dates ($t_{pass,s}$ and $t_{pass,a}$) expressed in days since 1 January of the respective season (Supplementary Table 2).

The Supplementary Information discusses in detail the potential effects on return rates introduced by seasonal differences in flight altitude and insect migration in the nocturnal boundary layer[3,53,54]. We find that each effect minimally changes the estimated seasonal biomass passages, biasing the return rates downward, at most by 4%.

Species composition. To assess which species groups predominantly contribute to our radar signals, we obtained breeding bird population estimates for the United States and Canada from the PIF Population Estimates Database for landbirds[24], supplemented with population size estimates for waterbirds and waders from the PIF Conservation Assessment Database[23] (with recent updates to population sizes provided by K.V.R.). We assessed for each species whether it was likely to migrate at night in the United States, following the migration status provided by PIF where available and complemented by an assessment by the authors (A.F. and K.V.R.) (see Supplementary Table 3). We gathered the average body mass per species from ref. [55] and took mass raised to the power (2/3) as a proportional measure of RCS. We estimated that 78% of the cross-sectional area of all nocturnally migrating birds in the United States combined are songbirds, and 22% are waterbirds and shorebirds. Supplementary Fig. 5 shows the cumulative distribution function of the cross-section values based on the PIF population estimates. It shows that 80% of the cross-sectional area is represented by birds with a body mass of less than 125 g, and 90% by birds smaller than 1 kg. These figures support our interpretation that the majority of the radar signals are caused by small songbirds, which is why our discussion of mortality and survival indices focuses on the songbird literature.

It is likely that the proportion of songbirds in our radar signals will be larger than the above estimates, because many waterbirds have (partly) overseas routes, and because these species also migrate during the day (especially geese and ducks), with radar signals from daylight hours not considered in our analyses. Very little migration was detected from November onwards (see Supplementary Video 2), which is when considerable waterfowl migration is expected, suggesting that waterfowl contributed relatively weakly to our estimates of migration passage.

To determine species composition of the assembly crossing each transect, and to compare our radar estimates of biomass passage with independent population estimates of migrating landbirds, we used information in the PIF Population Estimates Database[24] to determine landbird species (from Supplementary Table 3) with part or all of their populations migrating out of the contiguous United States in spring or autumn (that is, crossing the northern or southern transect, respectively). Because the PIF population estimates are for breeding adults only, our comparison is focused on spring migration passage, when the number of migrating individuals will be closest to the breeding population size. We used the percentage of the population that breeds in Canada and Alaska, or for short-distance migrants the percentage of the population wintering in the contiguous United States. To estimate the number of birds returning across the southern transect in spring, we used the percentage of the breeding population that winters on the Florida Peninsula or south of the United States in Latin America or the Caribbean.

We found that the total estimated spring passage of landbirds using this method (Supplementary Table 4) was similar to the biomass equivalent of passerine-sized birds estimated from the weather radar (2.68 versus 2.56 billion at the northern transect, and 2.46 versus 3.55 billion at the southern transect), suggesting that our quantification is biologically meaningful.

Migration distance. To estimate geographic characteristics of North American migratory bird distributions within the Western Hemisphere, we used range maps of species' breeding and winter distributions from NatureServe[56]. Following La Sorte[57], we converted range-map polygons to collections of equal-area hexagons of a global icosahedron[58] having a cell size of 12,452 km^2. We estimated the total migration distance between each species' breeding and winter ranges using the great circle (orthodromic) distance between the geographic centroids of the breeding and winter ranges, which were estimated by averaging the geographic locations of the hexagon cell-centres occurring within each species' breeding and winter ranges. We calculated the intersection of the great circle between breeding and wintering centroids with the transect and took the resulting segments as the distances travelled north (d_{north}) and south (d_{south}) of the transect. If breeding and non-breeding centroids were both positioned south of the transect, we took the distance travelled north of the transect to be zero, and the distance travelled south of the transect to be the full distance between the centroids. To determine assembly-averaged migration distances north and south of each transect (see Fig. 3), we calculated averages of species-specific line segment distances, weighed by the earlier-determined species population size crossing each transect, and by the average species mass[55] raised to the power (2/3) to account for RCS effects, resulting in $d_{north} = 1{,}396$ km and $d_{south} = 392$ for the north transect and $d_{north} = 1{,}512$ km and $d_{south} = 1{,}350$ km for the south transect. The result of a much longer d_{south} for the south transect is highly robust and remains when weighing only by population size (north transect: $d_{north} = 2{,}436$, $d_{south} = 539$; south transect: $d_{north} = 1{,}639$, $d_{south} = 1{,}726$), or when simply averaging over species without weighing (north transect: $d_{north} = 2{,}552$, $d_{south} = 368$; south transect: $d_{north} = 1{,}365$, $d_{south} = 1{,}370$). Furthermore, any small waterbird contribution to the biomass signal will reinforce the pattern further, as the majority of waterfowl winter at temperate latitudes within the United States, and most shorebirds crossing the southern transect tend to winter quite far south at tropical latitudes. We therefore expect the distances to be fairly robust against uncertainties in species composition, population size estimates and RCSs.

Statistics. Differences in seasonal transect passages were tested with linear mixed models using the R package lme4[59], with transect (north and south) as a fixed effect and year as a random effect. Two-sided P values for the fixed effect were calculated with a Wald chi-squared test, using the Anova function from the R package car[60]. Throughout the paper, values are reported as means ± s.d. over years.

Reporting Summary. Further information on research design is available in the Nature Research Reporting Summary linked to this article.

Data availability

NEXRAD weather radar data were accessed from the public 'noaanexrad-level2' Amazon S3 bucket[20] (https://aws.amazon.com/public-datasets/nexrad/).

Received: 19 February 2018; Accepted: 14 August 2018;
Published online: 17 September 2018

References

1. Hahn, S., Bauer, S. & Liechti, F. The natural link between Europe and Africa—2.1 billion birds on migration. *Oikos* **118**, 624–626 (2009).
2. Bauer, S. & Hoye, B. J. Migratory animals couple biodiversity and ecosystem functioning worldwide. *Science* **344**, 1242552 (2014).
3. Hu, G. et al. Mass seasonal bioflows of high-flying insect migrants. *Science* **354**, 1584–1587 (2016).
4. Holland, R. A., Wikelski, M. & Wilcove, D. S. How and why do insects migrate? *Science* **313**, 794–796 (2006).
5. Faaborg, J. et al. Conserving migratory landbirds in the New World: do we know enough? *Ecol. Appl.* **20**, 398–418 (2010).
6. Klaassen, R. et al. When and where does mortality occur in migratory birds? Direct evidence from long-term satellite tracking of raptors. *J. Anim. Ecol.* **83**, 176–184 (2014).
7. Sillett, T. S. & Holmes, R. T. Variation in survivorship of a migratory songbird throughout its annual cycle. *J. Anim. Ecol.* **71**, 296–308 (2002).
8. Faaborg, J. et al. Recent advances in understanding migration systems of New World land birds. *Ecol. Monogr.* **80**, 3–48 (2010).
9. Rushing, C. S. et al. Spatial and temporal drivers of avian population dynamics across the annual cycle. *Ecology* **98**, 2837–2850 (2017).
10. Wilcove, D. & Wikelski, M. Going, going, gone: is animal migration disappearing? *PLoS Biol.* **6**, 1361–1364 (2008).
11. La Sorte, F. A., Fink, D., Hochachka, W. M. & Kelling, S. Convergence of broad-scale migration strategies in terrestrial birds. *Proc. R. Soc. B* **283**, 20152588 (2016).
12. Webster, M. S., Marra, P. P., Haig, S. M., Bensch, S. & Holmes, R. T. Links between worlds: unraveling migratory connectivity. *Trends Ecol. Evol.* **17**, 76–83 (2002).
13. Sauer, J. R., Pendleton, G. W., Peterjohn, B. G. & Peterjohnt, B. G. Evaluating causes of population change in North American insectivorous songbirds. *Conserv. Biol.* **10**, 465–478 (1996).
14. Marra, P. P. Linking winter and summer events in a migratory bird by using stable-carbon isotopes. *Science* **282**, 1884–1886 (1998).
15. Anders, A. D. & Marshall, M. R. Increasing the accuracy of productivity and survival estimates in assembling landbird population status. *Conserv. Biol.* **19**, 66–74 (2005).
16. Lok, T., Overdijk, O. & Piersma, T. The cost of migration: spoonbills suffer higher mortality during trans-Saharan spring migrations only. *Biol. Lett.* **11**, 20140944 (2015).

17. Grüebler, M. U., Korner-Nievergelt, F. & Naef-Daenzer, B. Equal nonbreeding period survival in adults and juveniles of a long-distant migrant bird. *Ecol. Evol.* **4**, 756–765 (2014).
18. Crum, T. D. & Alberty, R. L. The WSR-88D and the WSR-88D Operational Support Facility. *Bull. Am. Meteorol. Soc.* **74**, 1669–1687 (1993).
19. Bauer, S. et al. From agricultural benefits to aviation safety: realizing the potential of continent-wide radar networks. *BioScience* **67**, 912–918 (2017).
20. Ansari, S. et al. Unlocking the potential of NEXRAD data through NOAA's Big Data Partnership. *Bull. Am. Meteorol. Soc.* **99**, 189–204 (2017).
21. Dokter, A. M. et al. Bird migration flight altitudes studied by a network of operational weather radars. *J. R. Soc. Interface* **8**, 30–43 (2011).
22. La Sorte, F. A., Fink, D., Hochachka, W. M., Delong, J. P. & Kelling, S. Spring phenology of ecological productivity contributes to the use of looped migration strategies by birds. *Proc. R. Soc. B* **281**, 20140984 (2014).
23. *Avian Conservation Assessment Database* (Partners in Flight, 2017); http://pif.birdconservancy.org/ACAD/
24. *PIF Population Estimates Database* (Partners in Flight Science Committee, 2013); http://pif.birdconservancy.org/PopEstimates
25. La Sorte, F. A. & Fink, D. Projected changes in prevailing winds for transatlantic migratory birds under global warming. *J. Anim. Ecol.* **86**, 273–284 (2017).
26. Faaborg, J. et al. Recent advances in understanding migration systems of New World land birds. *Ecol. Monogr.* **80**, 3–48 (2010).
27. Cody, M. L. A general theory of clutch size. *Evolution* **20**, 174–184 (1966).
28. Böhning-Gaese, K., Halbe, B., Lemoine, N. & Oberrath, R. Factors influencing the clutch size, number of broods and annual fecundity of North American and European land birds. *Evol. Ecol. Res.* **2**, 823–839 (2000).
29. Martin, T. E. Avian life history evolution in relation to nest sites, nest predation, and food. *Ecol. Monogr.* **65**, 101–127 (1995).
30. Schmidt, K. A., Rush, S. A. & Ostfeld, R. S. Wood thrush nest success and post-fledging survival across a temporal pulse of small mammal abundance in an oak forest. *J. Anim. Ecol.* **77**, 830–837 (2008).
31. Anders, A. D., Dearborn, D. C., Faaborg, J. & Thompson, F. R. Juvenile survival in a population of Neotropical migrant birds. *Conserv. Biol.* **11**, 698–707 (1997).
32. Vitz, A. C. & Rodewald, A. D. Influence of condition and habitat use on survival of post-fledging songbirds. *Condor* **113**, 400–411 (2011).
33. Saether, B., Bakke, O. & Mar, N. Avian life history variation and contribution of demographic traits to the population growth rate. *Ecology* **81**, 642–653 (2000).
34. Root, T. L. et al. Fingerprints of global warming on wild animals and plants. *Nature* **421**, 57–60 (2003).
35. Van Doren, B. M., Sheldon, D., Geevarghese, J., Hochachka, W. M. & Farnsworth, A. Autumn morning flights of migrant songbirds in the northeastern United States are linked to nocturnal migration and winds aloft. *Auk* **132**, 105–118 (2015).
36. Gaston, K. J., Visser, M. E. & Holker, F. The biological impacts of artificial light at night: the research challenge. *Phil. Trans. R. Soc. B* **370**, 20140133 (2015).
37. Loss, S. R., Will, T. & Marra, P. P. Direct mortality of birds from anthropogenic causes. *Annu. Rev. Ecol. Evol. Syst.* **46**, 99–120 (2015).
38. La Sorte, F. A. et al. Global change and the distributional dynamics of migratory bird populations wintering in Central America. *Glob. Change Biol.* **23**, 5284–5296 (2017).
39. Bringi, V. N. & Chandrasekar, V. *Polarimetric Doppler Weather Radar* (Cambridge Univ. Press, Cambridge, 2001).
40. Stepanian, P. M., Horton, K. G., Melnikov, V. M., Zrnić, D. S. & Gauthreaux, S. A. Dual-polarization radar products for biological applications. *Ecosphere* **7**, e01539 (2016).
41. Krajewski, W. F., Ntelekos, A. A. & Goska, R. A GIS-based methodology for the assessment of weather radar beam blockage in mountainous regions: two examples from the US NEXRAD network. *Comput. Geosci.* **32**, 283–302 (2006).
42. *USGS Small-Scale Dataset—100-Meter Resolution Elevation of the Conterminous United States 201212 TIFF* (U.S. Geological Survey, 2012); https://www.sciencebase.gov/catalog/item/581d0539e4b08da350d52552
43. Doviak, R. J. & Zrnić, D. S. *Doppler Radar and Weather Observations* (Academic Press, San Diego, 1993).
44. Haase, G. & Landelius, T. Dealiasing of Doppler radar velocities using a torus mapping. *J. Atmospheric Ocean. Technol.* **21**, 1566–1573 (2004).
45. Heistermann, M. et al. The emergence of open-source software for the weather radar community. *Bull. Am. Meteorol. Soc.* **96**, 117–128 (2015).
46. Sheldon, D. et al. Approximate Bayesian inference for reconstructing velocities of migrating birds from weather radar. In *Proc. 27th AAAI Conference on Artificial Intelligence* 1334–1340 (AAAI Press, 2013).
47. Waldteufel, P. & Corbin, H. On the analysis of single-Doppler radar data. *J. Appl. Meteorol.* **18**, 532–542 (1978).
48. Holleman, I. Quality control and verification of weather radar wind profiles. *J. Atmospheric Ocean. Technol.* **22**, 1541–1550 (2005).
49. Vaughn, C. R. Birds and insects as radar targets: a review. *Proc. IEEE* **73**, 205–227 (1985).
50. Merkel, D. Docker: lightweight Linux containers for consistent development and deployment. *Linux J.* **2014**, 2 (2014).
51. Alerstam, T. Flight by night or day? Optimal daily timing of bird migration. *J. Theor. Biol.* **258**, 530–536 (2009).
52. Pebesma, E. J. Multivariable geostatistics in S: the gstat package. *Comput. Geosci.* **30**, 683–691 (2004).
53. Westbrook, J. K. Noctuid migration in Texas within the nocturnal aeroecological boundary layer. *Integr. Comp. Biol.* **48**, 99–106 (2008).
54. Drake, V. A. & Reynolds, D. R. *Radar Entomology: Observing Insect Flight and Migration* (CABI, Wallingford, Boston, 2012).
55. Dunning, J. B. Jr *CRC Handbook of Avian Body Masses* 2nd edn (CRC Press, Boca Raton, 2008).
56. Ridgely, R. S. et al. *Digital Distribution Maps of the Birds of the Western Hemisphere* Version 3.0. (NatureServe, 2017).
57. La Sorte, F. A., Hochachka, W. M., Farnsworth, A., Dhondt, A. A. & Sheldon, D. The implications of mid-latitude climate extremes for North American migratory bird populations. *Ecosphere* **7**, e01261 (2016).
58. Sahr, K. Hexagonal discrete global grid systems for geospatial computing. *Arch. Photogramm. Cartogr. Remote Sens.* **22**, 363–376 (2011).
59. Bates, D., Mächler, M., Bolker, B. M. & Walker, S. C. Fitting linear mixed-effects models using lme4. *J. Stat. Softw.* **67**, 1–48 (2015).
60. Fox, J. & Weisberg, S. *An R Companion to Applied Regression* (Sage, Thousand Oaks, 2002).

Acknowledgements

This work was supported through a Rose Postdoctoral Fellowship (to A.M.D.), AWS Cloud Credits for Research (to A.M.D.), NSF ABI innovation DBI-1661259 (to A.M.D. and F.A.L.S.), the Leon Levy Foundation (to A.F. and D.F.), National Fish and Wildlife Foundation 6001.16.052172 (to A.F. and S.K.), NSF IIS-1633206 (to A.F. and S.K.), NSF ABI sustaining DBI-1356308 (to F.A.L.S., D.F. and S.K.) and the Wolf Creek Charitable Foundation (F.A.L.S.).

Author contributions

A.M.D., A.F. and S.K. conceived the study. A.M.D. performed the research and analysed the data. F.A.L.S. calculated species breeding and wintering distribution centroids. K.V.R. compiled transect species compositions from PIF population estimates. A.M.D. wrote the paper with input from all authors.

Competing interests

The authors declare no competing interests.

Additional information

Supplementary information is available for this paper at https://doi.org/10.1038/s41559-018-0666-4.

Reprints and permissions information is available at www.nature.com/reprints.

Correspondence and requests for materials should be addressed to A.M.D.

Publisher's note: Springer Nature remains neutral with regard to jurisdictional claims in published maps and institutional affiliations.

nature research

Corresponding author(s): Adriaan M. Dokter

Reporting Summary

Nature Research wishes to improve the reproducibility of the work that we publish. This form provides structure for consistency and transparency in reporting. For further information on Nature Research policies, see Authors & Referees and the Editorial Policy Checklist.

Statistical parameters

When statistical analyses are reported, confirm that the following items are present in the relevant location (e.g. figure legend, table legend, main text, or Methods section).

n/a	Confirmed	
☐	☒	The exact sample size (*n*) for each experimental group/condition, given as a discrete number and unit of measurement
☐	☒	An indication of whether measurements were taken from distinct samples or whether the same sample was measured repeatedly
☐	☒	The statistical test(s) used AND whether they are one- or two-sided *Only common tests should be described solely by name; describe more complex techniques in the Methods section.*
☐	☒	A description of all covariates tested
☐	☒	A description of any assumptions or corrections, such as tests of normality and adjustment for multiple comparisons
☐	☒	A full description of the statistics including central tendency (e.g. means) or other basic estimates (e.g. regression coefficient) AND variation (e.g. standard deviation) or associated estimates of uncertainty (e.g. confidence intervals)
☐	☒	For null hypothesis testing, the test statistic (e.g. *F*, *t*, *r*) with confidence intervals, effect sizes, degrees of freedom and *P* value noted *Give P values as exact values whenever suitable.*
☒	☐	For Bayesian analysis, information on the choice of priors and Markov chain Monte Carlo settings
☒	☐	For hierarchical and complex designs, identification of the appropriate level for tests and full reporting of outcomes
☐	☒	Estimates of effect sizes (e.g. Cohen's *d*, Pearson's *r*), indicating how they were calculated
☐	☒	Clearly defined error bars *State explicitly what error bars represent (e.g. SD, SE, CI)*

Our web collection on statistics for biologists may be useful.

Software and code

Policy information about availability of computer code

Data collection	n/a
Data analysis	We used the algorithm vol2bird (0.3.18) to extract bird information from weather radar data, as described in this publication: Dokter, A. M., Liechti, F., Stark, H., Delobbe, L., Tabary, P., & Holleman, I. (2010). Bird migration flight altitudes studied by a network of operational weather radars. Journal of the Royal Society Interface, rsif20100116. The code has been made available on Github: https://github.com/adokter/vol2bird As well in the R-package bioRad for analysing weather radar data: https://github.com/adokter/bioRad

For manuscripts utilizing custom algorithms or software that are central to the research but not yet described in published literature, software must be made available to editors/reviewers upon request. We strongly encourage code deposition in a community repository (e.g. GitHub). See the Nature Research guidelines for submitting code & software for further information.

Data

Policy information about availability of data

All manuscripts must include a data availability statement. This statement should provide the following information, where applicable:

- Accession codes, unique identifiers, or web links for publicly available datasets
- A list of figures that have associated raw data
- A description of any restrictions on data availability

NEXRAD weather radar data were accessed from the public “noaa-nexrad-level2” Amazon S3 bucket.

Field-specific reporting

Please select the best fit for your research. If you are not sure, read the appropriate sections before making your selection.

☐ Life sciences ☐ Behavioural & social sciences ☒ Ecological, evolutionary & environmental sciences

For a reference copy of the document with all sections, see nature.com/authors/policies/ReportingSummary-flat.pdf

Ecological, evolutionary & environmental sciences study design

All studies must disclose on these points even when the disclosure is negative.

Study description	We estimated continental biomass flows of nocturnal avian migrants across the contiguous U.S. using a network of 143 weather radars. Aerial biomass density was estimated from the radars' reflectivity product and biomass speed and direction from the radars' radial velocity product.
Research sample	Our research sample consisted of 143 radars across the US, each providing half-hourly data during 5 autumn seasons (2013-2017) and 4 spring seasons (2014-2017) during night time. Each half-hourly profile consisted of 20 200-m altitude bins (spanning 0-4 km above ground level)
Sampling strategy	Our choice of the autumn 2013 - autumn 2017 period was related to the availability of dual-polarization data, which was available only from autumn 2013 onwards for the full radar network.
Data collection	Data were used as provided by the US National Oceanic and Atmospheric Administration (NOAA)
Timing and spatial scale	Our choice of the autumn 2013 - autumn 2017 period was related to the availability of dual-polarization data, which was available only from autumn 2013 onwards for the full radar network. We restricted to half hourly profiles to calculate the seasonal total migration traffic across each station, as we found that higher resolution sampling (down to every 10 minutes) produced seasonal migration traffic estimates that were within 1% of when using half-hourly profiles.
Data exclusions	No data was excluded
Reproducibility	Our analysis is based on observational data, therefore experimental manipulation and replication is not applicable to our study
Randomization	Our analysis is based on observational data, therefore randomization is not applicable to our study
Blinding	Our analysis is based on observational data, therefore blinding is not applicable to our study

Did the study involve field work? ☐ Yes ☒ No

Reporting for specific materials, systems and methods

Materials & experimental systems

n/a	Involved in the study
☒	☐ Unique biological materials
☒	☐ Antibodies
☒	☐ Eukaryotic cell lines
☒	☐ Palaeontology
☒	☐ Animals and other organisms
☒	☐ Human research participants

Methods

n/a	Involved in the study
☒	☐ ChIP-seq
☒	☐ Flow cytometry
☒	☐ MRI-based neuroimaging